Molten Semiconductors for High Temperature Thermoelectricity

Citation: Zhao, Youyang et al. "Molten Semiconductors for High Temperature Thermoelectricity." ECS Journal of Solid State Science and Technology 6, 3 (December 5, 2016): N3010–N3016. © 2016 The Author(s)

As Published: http://dx.doi.org/10.1149/2.0031703JSS

Publisher: Electrochemical Society

Persistent URL: http://hdl.handle.net/1721.1/111652

Version: Final published version: final published article, as it appeared in a journal, conference proceedings, or other formally published context

JSS Focus Issue on Thermoelectric Materials & Devices

Molten Semiconductors for High Temperature Thermoelectricity

Youyang Zhao, Charles Rinzler, and Antoine Allanore*,z

Department of Materials Science & Engineering, Massachusetts Institute of Technology, Cambridge, Massachusetts 02139, USA

High temperature (>900°C) industrial waste heat recovery remains a key challenge for thermoelectric materials. The unique combination of high temperature, low heat-flux, and large surface area of waste heat generation as analyzed herein shows that active materials cost is the main metric inhibiting application. Molten compounds with semiconducting properties are therefore proposed as a cost-effective addition to solid-state materials for these conditions. A review of prior experimental results is presented, after which we demonstrate the performance of a laboratory-scale device based on molten SnS. The results allow reporting, for the first time, the Figure of Merit (ZT) and the conversion efficiency of the candidate materials. In addition, the Seebeck coefficient of molten SnS is reported. The results confirm the opportunity offered by molten thermoelectric compounds and allow discussion of the remaining materials and engineering challenges that need to be tackled in order to envision the future deployment of thermoelectric devices based on molten semiconductors.

Manuscript submitted September 22, 2016; revised manuscript received October 31, 2016. Published December 5, 2016. *This paper is part of the JSS Focus Issue on Thermoelectric Materials & Devices: Phonon Engineering, Advanced Materials and Thermal Transport.*

Industrial waste heat represents an important source of energy (around 5% of the total US annual energy production, i.e. 1,000,000 GWh), a significant fraction of it being generated at high temperature (around 20% of the industrial waste heat is at T > 650°C).[1] Because of such high exergy, there is an interest in directly recovering this energy in the form of electricity, potentially via thermoelectric conversion.

Though exceptional progress on solid-state materials for thermoelectrics has been accomplished, including extending their maximum range of operating temperature, there are to date no material systems and devices that have been implemented in the factories which generate this high quality waste heat.

We herein first analyze the cost and materials properties required to potentially enable such deployment. The analysis reveals that for large-scale (i.e. large surface of heat dissipation), low heat-flux and high temperature applications such as primary steel or glass production, the cost of the thermoelectric materials is the primary driver for materials choice. In addition, the heat-generating locations in the existing processes call for materials compatible with very high temperature. Finally, the chosen materials system will have to exhibit mechanical stability when subject to a large temperature difference at high temperature.

Additionally, a survey of the prior art and available data show that molten semiconductors are likely to fulfill the majority of the proposed criteria, suggesting the opportunity to complement solid-state materials to extend thermoelectricity to high-temperature industrial waste heat recovery.

Finally, the practical opportunity offered by molten thermoelectrics is demonstrated, and both experimental materials property data as well as performance of a laboratory-scale device are reported. The results enable the discussion of the remaining materials science and engineering challenges to allow further developments and future implementation.

High Temperature Waste Heat Sources, Challenges and Opportunity

For glass and primary steel production[a], more than 50% of the total waste heat is inherited from the highest-temperature and most energy-intensive operation, i.e. melting or reduction. Such operations are run in process units (namely a furnace or a reactor) the design of which, optimized for the target materials production, dictates the amount and temperature of the "wasted" heat-flux. Figure 1 shows schematically the location of the waste heat generation, its temperature and the corresponding heat-fluxes and surfaces through which high exergy waste heat is lost in primary steel production (blast furnace) or glass making.

The heat-fluxes lost from the reactors are characterized by a high temperature of generation - greater than 1000°C for a fraction of it; and even greater than 1500°C in certain locations. The surface areas involved are extremely large (more than 300 m^2), leading to relatively modest heat-fluxes, between 1 and 10 kW/m^2. One must acknowledge that such reactors have been optimized from a cost and energy efficiency perspective to match the cost of the final product (i.e. steel and glass). Therefore, the location of the heat losses and their temperature is unlikely to be modified in order to allow for their recovery. This reality has large consequences on the ability to implement thermoelectric materials and devices for high temperature industrial waste heat recovery, as shown hereafter.

Materials and Devices Challenges

As presented above, the temperature of the high exergy industrial waste heat represents a first critical challenge for the selection of candidate thermoelectric materials. Silicon-germanium can be considered the thermoelectric material with the highest temperature of operation (~1000°C) that has been implemented as a device[6–9] while other materials are still at the stage of discovery and development. The metric typically put forth to evaluate the heat-to-electricity conversion is the so-called "Figure of Merit" (ZT) given in the following Equation 1 as a function of Seebeck coefficient (α), electrical conductivity (σ) and thermal conductivity (κ).

$$ZT = \frac{\sigma\alpha^2}{\kappa}T \quad [1]$$

In the most realistic - and optimistic - scenario, ZT is around 1.[10]

The fraction of the heat that can be converted to electricity (i.e. thermoelectric efficiency) is then provided by the following Equation 2[9] given the Figure of Merit at average temperature ($Z\bar{T}$), hot-end

*Electrochemical Society Member.

zE-mail: allanore@mit.edu

[a]Fundamentals of materials processing suggest that the realities presented herein hold true for other metal smelting, cement production or incineration.

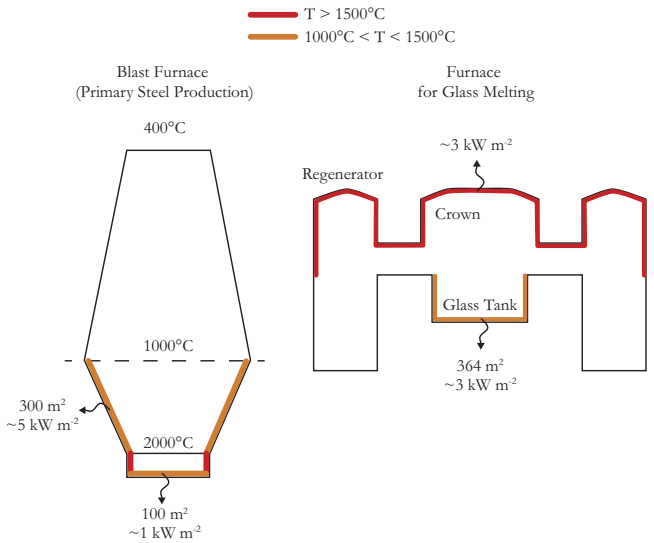

Figure 1. Schematic regions of generation and availability of high temperature waste heat in primary steel production (left)[2,3] and glass melting (right).[4,5] Not to scale.

temperature (T_H), and cold-end temperature (T_C):

$$\eta = \frac{T_H - T_C}{T_H} \frac{\sqrt{1 + Z\bar{T}} - 1}{\sqrt{1 + Z\bar{T}} + \frac{T_C}{T_H}} \quad [2]$$

The maximum power generated (P_{out}) is obtained from the thermoelectric voltage and the internal resistance of the thermoelectric material under the condition of impedance matching neglecting any contact resistance where x is the material thickness and A is the cross-sectional area:

$$P_{out} = \frac{(\alpha \Delta T)^2}{4 \cdot \frac{1}{\sigma} \cdot \frac{x}{A}} \quad [3]$$

Additional constraints apply for high temperature industrial waste heat. Large surface areas have to be covered calling for a material with scalable manufacturing. Relatively small heat-fluxes must be harvested and for a given material thermal conductivity (κ) and temperature difference (dT), the corresponding material thickness (dx) varies with heat-flux (q) following Fourier's Law,

$$q = -\kappa \frac{dT}{dx} \quad [4]$$

Equation 4 implies the need for a large material thickness when heat-flux is small.

Since the thermoelectric power is directly proportional to the square of the temperature difference, it is desirable to maximize the latter for thermoelectric generation. At the same time, a smaller material thickness helps reduce the active material and manufacturing costs. For a typical solid-state thermoelectric device designed to operate at a 400°C temperature difference (e.g. T_H = 500°C) with a material thermal conductivity of 2 W m^{-1} K^{-1} and a thickness of 1 cm, a minimum heat-flux of 80 kW m^{-2} is required to achieve steady-state based on Fourier's Law. The corresponding 400°C cm^{-1} temperature gradient is considered to date the upper limit of operations of solid-state thermoelectric devices beyond which mechanical stability is limiting. Indeed, a larger temperature difference can, for example, lead to cracking of the solid-state thermoelectric materials due to the corresponding amplitude of thermal stress. Additionally, the mismatch in coefficient of thermal expansion between the electrode (usually a metal) and the thermoelectric material (usually a non-metal) often leads to poor electrical and thermal contact.[11–16] In this context, harvesting heat-fluxes of 5 kW m^{-2} as experienced in high temperature industrial waste heat requires a thickness of 16 cm for a 400°C temperature difference. All these realities indicate that a large volume of material is required for high-temperature waste heat thermoelectricity, which justifies the quest for low-cost materials.

The metric of "dollar per watt of generated power", DPW, as put forth for renewable power generation, can be readily evaluated given the material volume (V) and volumetric price (M_{price}), only accounting the raw thermoelectric materials costs:

$$DPW = \frac{V M_{price}}{P_{out}} \quad [5]$$

Combining the maximum power output (Eq. 3) and the cost basis (Eq. 5) allows to evaluate DPW as a function of the magnitude of the heat-flux. The DPW evaluated on a materials basis is obtained via:

$$DPW = \frac{4\kappa^2 M_{price}}{\alpha^2 q^2 \sigma} \quad [6]$$

Figure 2 is a contour plot that shows DPW as a function of the magnitude of the input heat-flux and the volumetric material cost assuming a ZT of 1 and a thermal conductivity of 2 W m^{-1} K^{-1}. The plot shows that a promising solid-state material such as bismuth telluride, at approximately \$10^6 m^{-3}, requires a flux of around 90 kW m^{-2} in order to achieve a cost basis of \$1 W^{-1}.

This analysis corroborates the results presented previously for mid-temperature range waste heat recovery calling for a revolution in solid-state materials discovery and engineering for large temperature difference, low-heat-flux waste heat recovery.[17] In our opinion, a novel class of non-solid-state materials could be considered in order to harvest the industrial waste heat discussed above, materials that have a high temperature of operation and a low volumetric cost compared to their solid-state counterparts. For the waste heat-fluxes encountered in primary operations of steel and glass industry, a material cost ranging from \$ 10,000 m^{-3} to \$60,000 m^{-3} is required for heat-fluxes of no more than 10 kW m^{-2} in order to achieve \$1 W^{-1} to \$5 W^{-1} materials cost basis. Hereafter presented and discussed are molten semiconductors which, according to their bulk price, are potential candidates for such thermoelectric application.

Opportunity Offered by Molten Semiconductors

Molten semiconductors, as opposed to their solid-state counterparts, have high operating temperatures and low material costs as shown in Table I. The materials cost are estimated here following the approach developed previously by Yadav,[18] i.e. using elemental

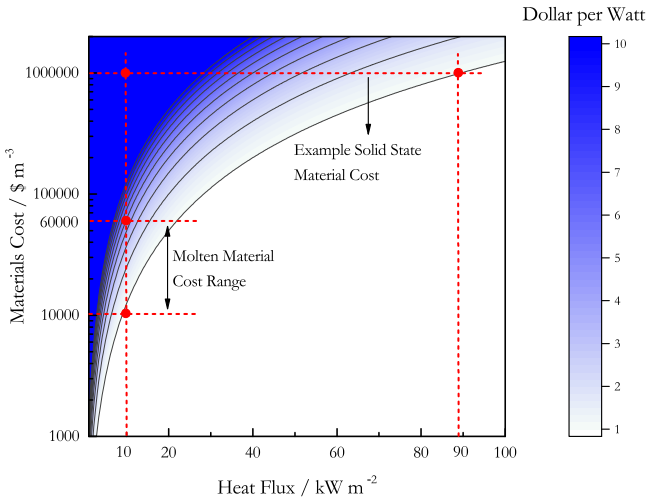

Figure 2. Variation of cost per watt of power generated, (DPW, color gradient), with the thermoelectric materials volumetric cost and the magnitude of the heat-flux of the heat source. At a given heat-flux, DPW increases linearly with material cost. The dots at the intersections of the dash lines give approximate DPW for materials with different costs and at different heat-fluxes.

Table I. Physical properties and material cost of selected molten semiconductors.

Ref.	Material System	Physical Properties* Seebeck ($\mu V\ K^{-1}$)	Electrical Conductivity ($S\ m^{-1}$)	Thermal Conductivity ($W\ m^{-1}\ K^{-1}$)	Melting Point (°C)	Figure of Merit ZT	Cost** ($\$\ m^{-3}$)
24–27	Te_xTl_{1-x}	−150	5×10^4	1.2	420	0.67 at 477°C	47,000,000
26,28	Te_xSe_{1-x}	65	3.3×10^4	2.2	430	0.06 at 435°C	546,000
21,29	Ni_3S_2	35	5×10^5	NA	800	NA	54,000
30,31	Ag_2S	NA	2×10^4	0.8	842	NA	3,200,000
19,20,32	SnS	−200	4×10^3	NA	882	NA	65,000
21	Co_4S_3	NA	4×10^5	NA	920	NA	115,000
33,34	$Cu_2S_{0.25}Te_{0.75}$	180	2.5×10^4	1.5	1000	0.7 at 1070°C	225,000
30,32	PbS	−200	2.2×10^4	NA	1120	NA	13,500
22,30,35	Cu_2S	335	$8 \times 10^3 - 1 \times 10^4$	0.8-1.4	1130	1 at 1130°C	27,400

*Physical properties shown here are for the specific temperature and composition that lead to the highest Figure of Merit for the system.
**Price for elements obtained from U. S. Geological Survey.[36]

basis costs. Indeed, the most common synthesis route to obtain molten semiconductors is by mixing the pure components at the desired ratio prior to a melting process.[19–23]

Molten semiconductors attracted great research interest in the late 1950s and 1960s. Two fundamental ideas have shaped the knowledge of molten semiconductors. First, the introduction of the pseudo-gap theory by Mott[37] postulated a "band structure" for liquids based on their retention of solid-state short-range order. Second, the relationship between retention of solid-state short-range order and semiconducting properties was proposed by Ioffe and Regel.[38] Both concepts opened a new research horizon for disordered semiconducting phases. Applying semiconducting properties of liquids, especially of high melting point melts, to thermoelectric conversion at high temperature is one application that drew research attention.

In the 1960s, a few pioneer works experimentally measured thermoelectric properties of molten chalcogenide systems. Cutler and Mallon[24,25,27,28] focused on tellurium (Te)-based systems with addition of selenium (Se) and thallium (Tl). High temperature data for the Seebeck coefficient and electrical conductivity along with theoretical calculation of thermal conductivity provided some of the first Figures of Merit for molten semiconductor systems. Other Te- and Se-based binary systems have also been investigated. Belotskii and Manik[30] gave a comprehensive summary of the thermoelectric properties available for molten systems to date. Another well-studied example system is cuprous sulfide (Cu_2S), with its earliest electrical conductivity study by Bourgon, Derge and Pound[22] justifying its classification as a semiconductor. Molten Cu-S and its derivatives were later extensively studied by Johnson and Readal.[33–35,39,40] They also pioneered the experimental measurement of thermal conductivity in the molten state. Due to experimental difficulties such as heat flow management and the complexity of thermal conduction (e.g. possible presence of bipolar conduction), the experimental error remains of the order of ±25%, a remarkable result considering the temperature of operation. With a p-type Seebeck coefficient greater than 300 $\mu V\ K^{-1}$, Cu_2S is considered one of the most promising molten semiconductors for thermoelectric application, with a Figure of Merit close to unity.

As shown in Table I, other molten sulfide systems that also exhibit semiconducting properties such as Ni-S, Co-S, Sn-S, Ag-S, Pb-S[19–21,29,30] are of interest from both a cost and performance perspective. Unfortunately, a dearth of experimental or modeling physical and chemical property data currently limits our ability to further support the development of molten sulfides as potential thermoelectric materials. Among these systems, SnS and PbS were reported to have very promising Seebeck coefficient.[32] In addition, their n-type Seebeck opens the possibility to constructing a p-n pair with Cu_2S. Some results remain puzzling from a materials science perspective, such as the reported trend of SnS Seebeck with temperature in the molten state.[32]

However, for most of the promising molten semiconductor systems including SnS and PbS, the thermal conductivity remains unknown. It is anticipated that the electronic thermal conductivity (as calculated from Wiedemann-Franz law) is valid and that the molecular contribution to thermal conductivity of the molten semiconductors is negligible.[41] Williams et al.[42] investigated the heat-transfer inside molten Ag-S system with a concentric cylinder device. By studying the relation between the apparent thermal conductivity of the melt and the cell dimension, they conclude that liquid convection is a major heat-transfer mechanism. Assuming molten sulfides in general have similar thermal and fluid dynamics properties,[43] the same conclusion is likely to be applicable to other molten sulfide systems.

We herein construct a thermoelectric test cell that adopts the similar concentric cylinder design put forth by Williams[42] at that time to investigate the thermal conductivity of molten Ag-S system and the possible role of convective heat-transfer. With the test cell, we demonstrate for the first time a lab-scale thermoelectric power generation using molten semiconductor (in this case SnS) operating in the temperature range of 950–1074°C. In addition to reporting the Figure of Merit (ZT) and the thermoelectric conversion efficiency of a laboratory device, the study demonstrates that the test-device will enable the evaluation of the intrinsic properties of new molten semiconductor candidate materials. It also substantiates the potential advantages and the remaining challenges for molten semiconductors to be deployed for high temperature industrial waste heat recovery.

Experimental

Thermoelectric material preparation.—Tin (99.85% metals basis, <150 μm, Sigma Aldrich) and Sulfur (99.5%, Sigma Aldrich) powders were mixed in a plastic weigh pan at 1:1 atomic ratio. The mixture was transferred to a graphite annulus-shaped crucible of 25.4 mm inner, 35.6 mm outer diameter and 30.5 mm height. The mixture and crucible were then sealed in a stainless steel 304 synthesis reactor with tungsten inert gas (TIG) welding. The whole process was performed under industrial grade argon atmosphere (Ar 99.998%, Airgas). The synthesis reactor was then transferred to a vertical tube furnace (CF56622C, Lindberg Blue M) with flowing Ar atmosphere (ultra-high purity, Airgas). After 20 min of Ar purging, the furnace temperature was raised from room temperature to 250°C at 5°C min^{-1} and maintained at 250°C for 3 hours to assure complete reaction between molten sulfur and molten tin. The furnace temperature was subsequently raised to 920°C at 5°C min^{-1} and maintained at 920°C for 1 hour to guarantee a fully molten reaction product, SnS. The furnace was cooled to room temperature at the natural cooling rate. After synthesis, the reactor was cut open and the condensed SnS was transferred to a dry box for storage under nitrogen (N_2) atmosphere (high purity, Airgas).

Thermoelectric test cell assembly.—The thermoelectric test cell, schematically presented in Figure 3, adopted a concentric cylinder geometry inspired by the work of Williams et al.[42] with a unileg

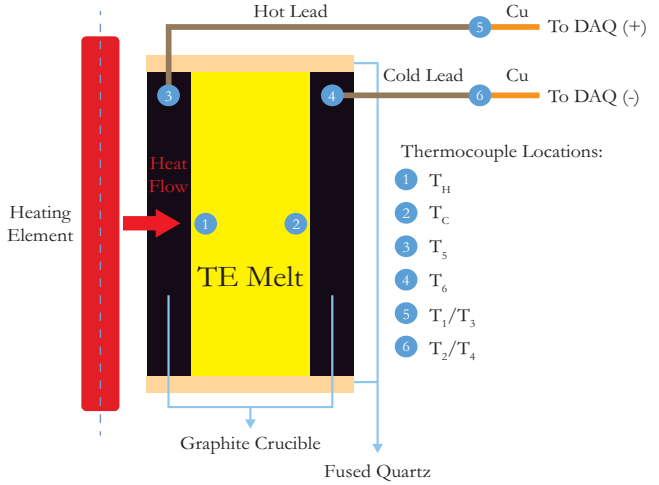

Figure 3. Schematic of the thermoelectric test cell, with the location of the melt, graphite crucible, fused quartz, primary/secondary leads, heating element, temperature measurement and lead connections. The dashed line locates the axisymmetry of the device.

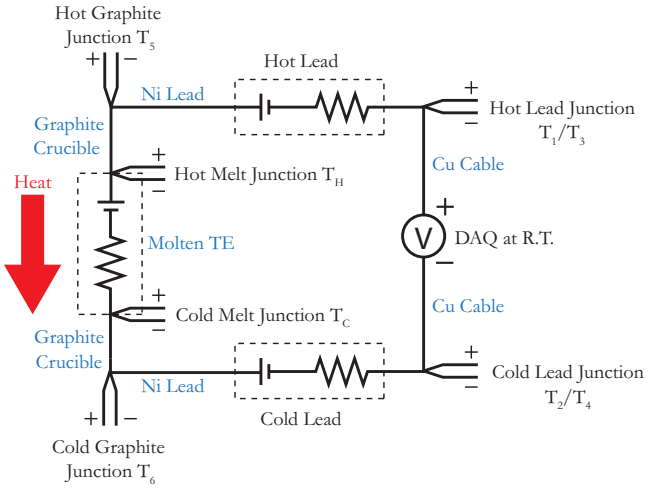

Figure 4. Electrical circuit showing the locations of temperature measurements and thermoelectric voltage. Impedance contributions from the thermoelectric melt, graphite crucible, and primary/secondary leads are shown. Only one circuit (i.e. primary) is shown. The circuits for primary and secondary leads are in parallel and share the same graphite crucible. Blue text specifies the materials of each section of the circuit. Contributions from graphite crucible and Cu cables are ignored due to their negligible temperature difference and/or low Seebeck coefficient.

design since only one type of thermoelectric melt (p- or n-type) was used. Electrical Discharge Machining (EDM) grade graphite (EC-15 ultrafine grain, Tokai Carbon) and a polished fused quartz plate (1.57 mm thickness, GE124 fused quartz) were used. Graphite served as both the crucible and electrodes. The fused quartz plate was joined to the graphite crucible with carbon paste (PELCO High Temperature Carbon Paste, Ted Pella Inc.) to ensure liquid containment (see Figure 3). Nickel rods (Ni 200, 6.35 mm diameter, McMaster-Carr) were cut into segments of 76.2 mm length and threaded to the graphite crucible to act as primary electrical leads. A total of 16 leads, 8 for each polarity, were placed in a radial symmetry to ensure uniform current distribution during power generation. Two graphite rods (EC-15 ultrafine grain, 3.17 mm diameter, Tokai Carbon) were connected to the graphite crucible with carbon paste to act as secondary leads. Type-K thermocouples (Omega) were used to measure the temperature at the lead junctions (T_1/T_2 and T_3/T_4 respectively for the primary and secondary leads). The leads were connected to a data acquisition system for voltage probing (OMB-DAQ-54, Omega). Four type-R thermocouples (Omega) shielded in fused quartz tubes were used for temperature measurement; two of which were inserted into the graphite crucible (T5 and T6) and the other two plunged into the SnS melt (T_H and T_C). The entire test cell was insulated with ceramic fiber blanket (at least 50 mm thick, Durablanket S, Unifrax). A SiC heating element (Henan J. K. Industry Co.) with 76.2 mm hot zone located at the center of the test cell acted as the heat source, with a total height that extended 22.9 mm above and below the graphite crucible. Four cooling fans were used to cool the outermost shell of the test cell.

Operation.—The thermoelectric test cell was transferred to a glove box filled with Ar (industrial grade, Airgas). The oxygen partial pressure (<200 ppm) was checked by an oxygen sensor prior to each experiment (Rapidox 3100, Cambridge Sensotec). A variable transformer (3PN2210B-DAM, ISE Inc.) with digital ammeter served as the power source and displayed the current through the heating element. A digital multimeter (197, Keithley) was used to measure the voltage across the heating element to determine the total electrical power input. Given the extension of the heating element (22.9 mm) above and below the crucible as guard heaters, a minimal edge effect due to axial heat flow is assumed in the hot-zone which is a well-accepted assumption with concentric cylinder cell design for thermal conductivity measurement. The heat flow through the molten material is then estimated as the total electrical power multiplied by the ratio of the height of the molten material to that of the hot zone of the heating element (e.g. approximately 0.4 in the test cell). The thermoelectric voltage from both the primary and secondary leads were continuously measured at 1 Hz using a multi-channel data acquisition system (OMB-DAQ-54, Omega). The heating power was controlled to slowly heat SnS to different temperature profiles, i.e. hot-end temperature (T_H) and cold-end temperature (T_C). A potentiostat (Reference 3000, Gamry) was used to perform electrochemical impedance spectroscopy (EIS) and linear sweep voltammetry (LSV) for each steady-state temperature profile. The temperature inside the glove box was continuously measured with a type-K thermocouple

Seebeck coefficient measurement.—The thermoelectric voltage measured at the primary and secondary leads included contribution from the melt, graphite crucible, lead materials and the copper measuring cables. The literature Seebeck coefficient for graphite, nickel, and copper along with the measured junction temperature (shown in Figure 4) were used to subtract these contributions.

Thermal conductivity estimation.—The apparent thermal conductivity of the melt is estimated based on the definition of the Figure of Merit (Eq. 1) given the experimental Seebeck coefficient and the literature electrical conductivity data. The Figure of Merit is back-calculated from Equation 2 given the experimental efficiency (η_{exp}) as follows,

$$\eta_{exp} = \frac{P_{out}}{0.4 Q_{total}} \quad [7]$$

where Q_{total} is the total electrical power input, the factor 0.4 is the ratio of the height of the molten material to that of the hot zone of the heating element introduced before (i.e. the denominator $0.4Q_{total}$ means 40% of the total heat generated by the heating element goes through the molten material given the condition of minimum axial heat flow in the hot-zone warranted by the presence of the guard heaters) and P_{out} is the electrical power generated by the melt after excluding the contribution from graphite, nickel and copper. The thermal conductivity due to natural convection is estimated based on the study by Williams et al.[42] who showed a linear relationship between the total apparent thermal conductivity and the cell dimension. We therefore obtained the apparent thermal conductivity of molten SnS by extrapolating the thermal conductivity due to natural convection from Williams et al. to the dimension of our test cell. Limited information[31,33] shows that the intrinsic thermal conductivities of molten sulfides are approximately

Table II. Summary of errors associated with measurement instrument and property data from literature used for uncertainty analysis.

Property	Error	Source/assumption
Temperature	0.25%	Thermocouple Specification
Voltage	−200 μV	Calibration against 1 mΩ resistor
Current	±5 pA ±0.05% of range ±0.2% of value	Potentiostat Specification
Seebeck Coefficient	0.3–3%	Standard deviation of measurements from present work
Electrical Conductivity	5%	Assumption based on limited information from literature

1 to 2 W m^{-1} K^{-1}. To simplify analysis, we assume the intrinsic thermal conductivity of molten SnS falls into the same range.

Uncertainty analysis.—Error propagation was adopted for uncertainty analysis after defining measurement errors from instruments and uncertainties for literature data. Assumptions were made if there was no available information. Table II summarizes the values and assumptions for the errors used for uncertainty analysis.

Results

Figure 5a represents the device voltage and power response to current measured by LSV for a hot-end temperature ranging from 951°C to 1074°C, with an average temperature difference of around 55°C. Figure 5b shows the maximum device power measured as a function of the hot-end temperature, from melting point up to 1074°C, during the course of over four hours of experiment.

Figure 6 shows the corresponding materials properties evaluated by subtracting the contribution from the graphite crucible, nickel leads and copper cables. Figure 6a shows a negative Seebeck coefficient for molten SnS of the order of 150–190 μV K^{-1} in magnitude, decreasing with temperature. This Seebeck is in the range reported by prior works for similar molten semiconductors (see Table I). Figure 6b shows an increase of the maximum melt power calculated with the electrical conductivity of molten SnS reported previously.[19] The Figure of Merit in Figure 6b is evaluated from Equation 2 and Equation 7, using the Seebeck coefficient measured in the present work, the literature electrical conductivity, and the experimental efficiency. It should be clarified that this Figure of Merit represents the molten material itself present inside a device and is obtained based on the maximum power generated by the melt alone (Figure 6b, black squares) after excluding device-level contributions (e.g. power and resistance from graphite, nickel and copper) instead of the maximum power generated at the device level (Figure 5b).

Figure 7 shows a slightly increasing experimental efficiency (η_{exp}) with temperature at the device level for molten SnS. Very reproducible efficiency data are observed during thermal cycling of the material over four hours of high-temperature operation. The efficiency predicted from materials properties and apparent thermal conductivity ("calculated efficiency") also shows an increasing trend with temperature.

The apparent thermal conductivity of SnS melt is evaluated in the range 4 to 6 W m^{-1} K^{-1} from the Figure of Merit data (Figure 6b). Using the extrapolation procedure discussed in the Experimental section, an effective thermal conductivity due to natural convection of around 3 W m^{-1} K^{-1} is obtained for molten SnS in our test cell. This convective thermal conductivity estimate seems to be sufficient to bridge the difference between the measured apparent thermal conductivity in our SnS experiment (≈4–6 W m^{-1} K^{-1}) and the expected intrinsic materials thermal conductivity (≈1–2 W m^{-1} K^{-1}).

Discussion

The Seebeck coefficient of SnS in the molten state reported in Figure 6a is of the same order of magnitude as in the prior art.[32] Its magnitude confirms retention of short-range order at melting and hence semiconducting properties in the molten state.[38] As a reference, solid-state SnS is reported to be a p-type semiconductor with a maximum Seebeck of +650 μV K^{-1} at around 350°C.[44–46] The experimental error of less than 6 μV K^{-1} in our data indicates that reliable Seebeck coefficient measurement for molten sulfides can be obtained with the thermoelectric device developed for this study, independent of the materials chosen for the voltage leads.

The decreasing Seebeck coefficient with temperature in the molten state reported in Figure 6a is in agreement with Mott's pseudo-gap model for disordered structures, where short-range order decreases with temperature which leads to a reduced effective bandgap. Previously reported data on the Seebeck of SnS did not exhibit this agreement with theory.[32]

The reproducibility of the Seebeck coefficient measurement across several thermal cycles and within a temperature range of approximately 200°C above the material melting point over the course of four hours of experiment is a unique feature of molten semiconductors. Molten SnS in the temperature window of 880°C to 1074°C is very stable and can undergo electronic and structural changes that are reversible. In particular, the reproducibility during heating and cooling indicates limited vaporization and limited composition change.

No hysteresis on the maximum device power (Figure 5b) is observed after more than four hours of experiment at high temperature, highlighting remarkably stable performance at the device level. There was no mechanical degradation found at the melt/electrode interface during post-test cell inspection. There is also no significant change in electrical conductivity observed during operation suggesting an acceptable wetting behavior between molten SnS and the graphite electrode regardless of thermal expansion. The ability to conform and wet to the contour of the graphite electrode indicates that devices based on molten thermoelectric materials exhibit electrical and mechanical robustness inherently sufficient to consider their usage in high temperature thermoelectric generators. The selected device design and construction materials prove a reliable platform for the study of both molten material properties and the efficiency of power generation at the device-level. Such reliable device design is foreseen as a key step for future scale-up studies.

The seemingly contradictory trend with temperature for maximum device power (Figure 5b) and maximum melt power (Figure 6b) is worth noting. The construction of the test cell used nickel as lead material which has an n-type Seebeck coefficient (the same as that of molten SnS) that increases in magnitude with temperature leading to more cancellation of thermoelectric voltage generated by molten SnS at higher temperature. The electrical resistivity of nickel also increases with temperature which causes increased internal resistance of the test cell. Overall, the performance at the device level decreases with temperature (i.e. decreasing device power in Figure 5b) due to negative impact from nickel leads regardless of the increasing performance of the melt with temperature (i.e. increasing melt power in Figure 6b).

The calculated efficiency presented in Figure 7 increases with temperature more than the experimental efficiency, most likely due to the assumption of a constant apparent thermal conductivity of 4 W m^{-1} K^{-1}. The results from the apparent and convective thermal conductivity estimates validate two assumptions; 1) molten SnS shares similar fluid dynamics behavior as the Ag-S system and 2) the major mode of heat-transfer in our experiment is likely natural convection. However, due to the lack of temperature-dependent study by Williams et al.[42] further analysis is limited at the moment. Realistically, taking into account the increase of apparent thermal conductivity with temperature will bring the calculated efficiency toward the experimental efficiency, which are already in reasonable agreement at low temperature. Beyond

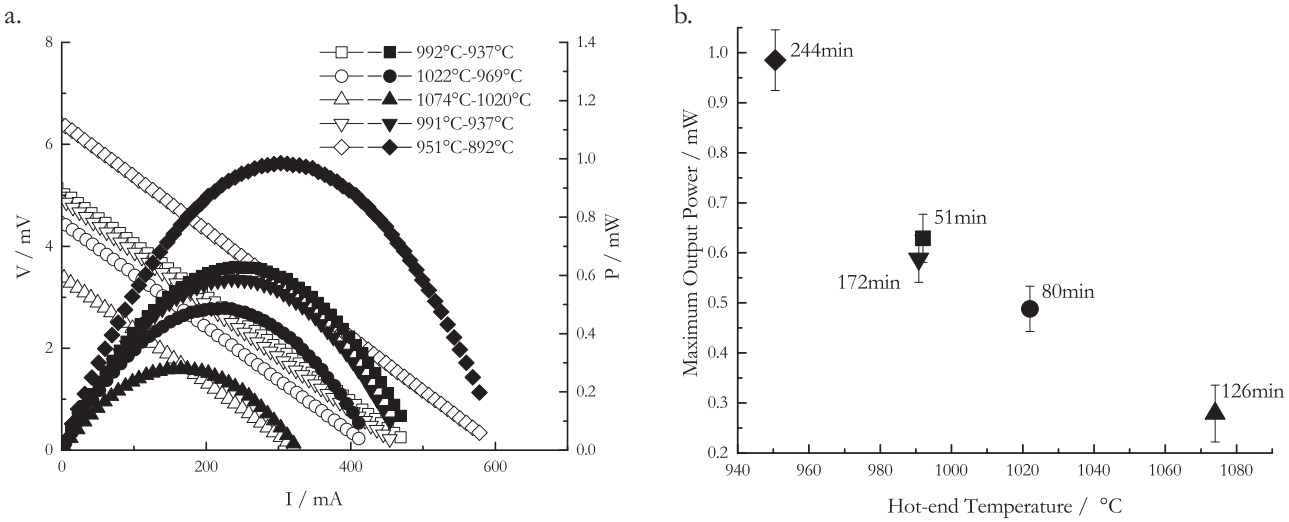

Figure 5. (a) Variation of the device voltage (V, open mark, left axis), and power (P, solid mark, right axis) with the current (I) for five different temperature profiles with an average temperature difference of around 55°C. (b) Maximum output power of the device, measured for each temperature profile, as a function of the hot-end temperature. Data were taken over the course of four hours of experiment when the material was thermally cycled over a range of 200°C above melting point.

the uncertainty associated with thermal conductivity, the results prove that electricity is indeed generated by the molten material inside the thermoelectric test cell. In addition, it suggests that the experimental method followed to subtract the lead materials contribution from the molten material is reliable. Finally, it shows that limited chemical interaction between the device and the thermoelectric material occurred such that the molten material is exhibiting performances approaching its theoretical limit.

In agreement with the predictions and analyses presented in the introduction, devices based on molten semiconductors will exhibit a material cost (i.e. excluding manufacturing cost) that is one to two orders of magnitude lower than their solid-state materials counterpart. Taking into account the ease of manufacturing, the synthesis method for SnS (see Experimental section) proves very flexible in terms of final geometry and dimension of material. The simplicity indicates a simple path to produce a thermoelectric material with large material thickness, in contrast to the challenges reported for the manufacturing of large-dimension solid-state materials.

Despite the promising thermoelectric properties of molten SnS and the stable device operation demonstrated in this work, the future deployment of molten thermoelectrics for high temperature waste heat recovery requires tackling open materials and engineering questions, discussed hereafter.

Envisioning a unicouple thermoelectric cell design (i.e. using both p- and n-type semiconductors) will require using materials with peak performance in the same temperature range. Otherwise, it might be more economically advantageous to adopt a unileg cell design.[47] The present and previous studies have identified several promising candidate materials (e.g. Cu_2S, SnS, and PbS) which are all binary systems, but their Seebeck performances and optimum temperature range of operation are potentially too dissimilar to allow their coupling. However, it has been demonstrated that a binary molten material system with small composition variation around a stoichiometric compound could exhibit both p- and n-type characteristics,[24,28,43,48] enabling the potential use of the same materials for both legs of a cell. In addition, the evolution of the fundamental properties of binaries upon addition

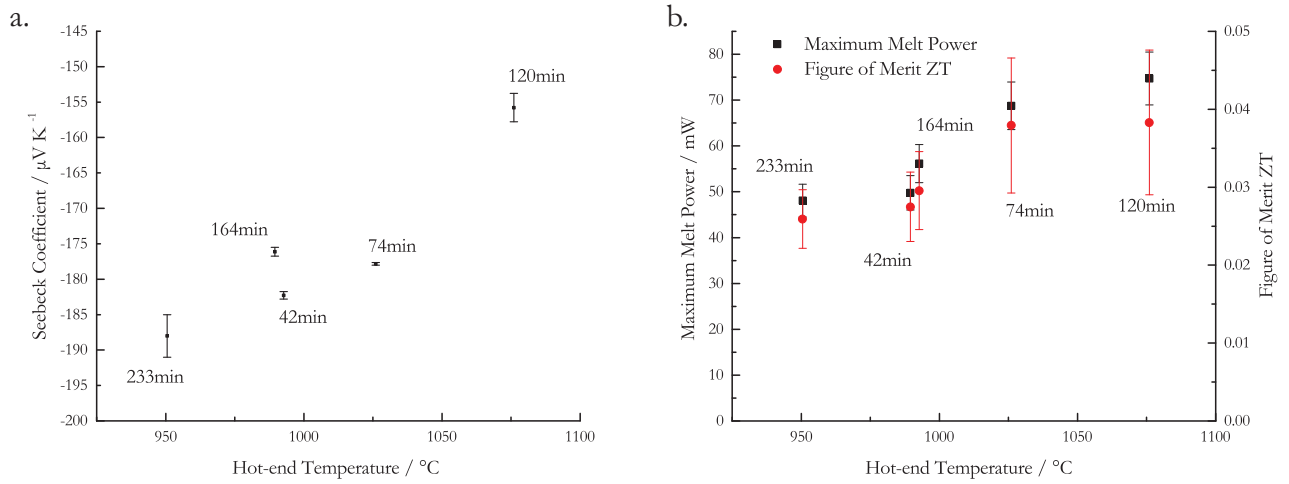

Figure 6. (a) Variation of the experimental Seebeck coefficient of molten SnS with the hot-end temperature during four hours of experiment at temperatures up to 1074°C. Error bars indicate ±1 standard deviations from the mean based on measurements from both primary and secondary leads after subtracting the lead contribution. (b) Variation of the maximum melt power (black squares, left axis), after subtracting lead contribution, and Figure of Merit (red circles, right axis) with hot-end temperature during four hours of experiment.

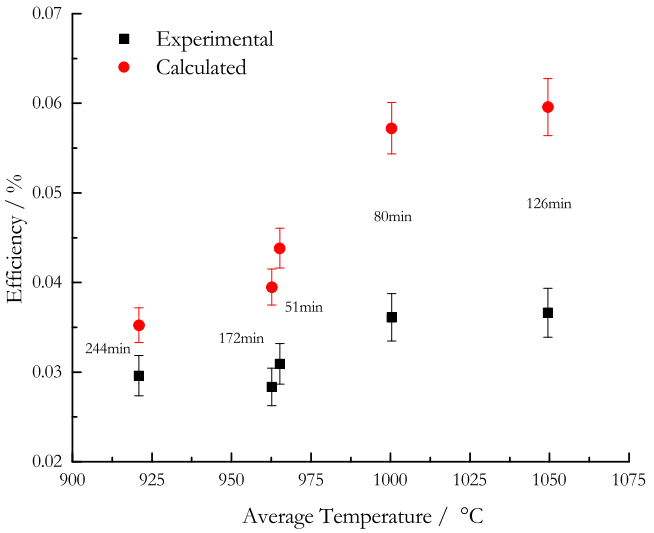

Figure 7. Variation of the experimental and the calculated efficiency for molten SnS as a function of the average melt temperature, at an average temperature difference of approximately 55°C. The calculated efficiency is obtained assuming a temperature-independent apparent thermal conductivity of 4 W m^{-1} K^{-1} which is the sum of the expected intrinsic materials thermal conductivity for molten sulfides[31,33] (≈1–2 W m^{-1} K^{-1}) and the effective thermal conductivity due to natural convection (explained in Discussion section) based on the analysis of Williams et al.[42]

of a third component (e.g. a mixture of Cu-Sn-S in the molten state) remains largely unknown, including and starting with their liquidus. It is therefore important to further study the fundamental materials properties of molten semiconductors to broaden the spectrum of materials selection and ultimately enable large-scale application.

Molten semiconductors are confirmed to be sufficiently low-cost materials to allow application at large scales and potentially harvest the low heat-flux waste heat generated by industrial processes. One critical challenge associated with applying large volumes of molten materials, or more precisely a large thickness, is the onset of convective heat-transfer. The efficiency results (Figure 7) and the thermal conductivity estimates have several implications regarding future improvements. First, given the confidence in Seebeck coefficient and electrical conductivity data, the uncertainty on the apparent thermal conductivity, especially the quantification of the contribution from natural convection, prevents accurate prediction of the thermoelectric performance of molten sulfides. Second, comparing the magnitude of the estimated thermal conductivity due to natural convection (≈3 W m^{-1} K^{-1}) with the expected intrinsic thermal conductivity for molten sulfides (1-2 W m^{-1} K^{-1}) shows that the management of natural convection inside the semiconductor melt offers the largest potential to improve the overall thermoelectric efficiency of a molten thermoelectric generation device. The practical upper limit of the thermoelectric conversion is hence most likely no longer determined by the intrinsic material thermal conductivity as in the case of solid-state thermoelectrics. It proves challenging, however, to quantify the convective heat-transfer with molten semiconductors due to the lack of material properties such as density, viscosity or thermal diffusivity. Other heat conduction mechanisms arising at high temperature may complicate the analysis of heat-transfer. For example, bipolar thermal conduction as described by solid-state physics,[49–51] first discovered in solid bismuth telluride,[52] may be present in molten semiconductors as well.[33]

Therefore, the frontiers in materials science and engineering of molten semiconductors reside in the ability to predict thermodynamics (e.g. quantitatively connecting thermodynamic mixing properties to the electronic properties of molten systems[53]) and transport properties in order to envision novel compositions with higher intrinsic thermoelectric properties as well as the design of large-scale devices that help mitigate natural convection.

References

1. T. Hendricks and W. T. Choate, *Engineering Scoping Study of Thermoelectric Generator Systems for Industrial Waste Heat Recovery*, U.S. Depart. of Energy, (2006).
2. G. Danloy, J. Mignon, R. Munnix, G. Dauwels, and L. Bonte, in *60th Ironmaking Conference Proceedings*, p. 37, Baltimore (2001).
3. S. Kumar, *ISIJ Int.*, **45**, 1122 (2005).
4. M. Lindig, *Glas. Technol.*, **46**, 109 (2005).
5. K. Khoshmanesh, A. Z. Kouzani, S. Nahavandi, and A. Abbassi, in *TENCON 2007 - IEEE Region 10 Conference*, p. 1, Taipei (2007).
6. K. Ikoma, M. Munekiyo, K. Furuya, M. Kobayashi, T. Izumi, and K. Shinohara, in *Proceedings of 17th International Conference on Thermoelectrics (ICT1998)*, p. 464 (1998).
7. X. W. Wang, H. Lee, Y. C. Lan, G. H. Zhu, G. Joshi, D. Z. Wang, J. Yang, A. J. Muto, M. Y. Tang, J. Klatsky, S. Song, M. S. Dresselhaus, G. Chen, and Z. F. Ren, *Appl. Phys. Lett.*, **93**, 193121 (2008).
8. H. J. Kim, Y. Park, G. C. King, K. Lee, and S. H. Choi, in *Material Research Society Fall Meeting* (2010).
9. S. W. Angrist, *Direct Energy Conversion*, 3rd ed., Allyn and Bacon, Boston, (1976).
10. C. B. Vining, *Nat. Mater.*, **8**, 83 (2009).
11. H. T. Kaibe, L. Rauscher, S. Fujimoto, T. Kurosawa, T. Kanda, M. Mukoujima, I. Aoyama, H. Ishimabushi, K. Ishida, and S. Sano, in *Proceedings of 23rd International Conference on Thermoelectrics (ICT2004)*, Adelaid, Australia (2004).
12. W. Shin, N. Murayama, K. Ikeda, and S. Sago, *J. Power Sources*, **103**, 80 (2001).
13. R. Funahashi, M. Mikami, T. Mihara, S. Urata, and N. Ando, *J. Appl. Phys.*, **99**, 66117 (2006).
14. T. C. Harman, R. E. Reeder, M. P. Walsh, B. E. LaForge, C. D. Hoyt, and G. W. Turner, *Appl. Phys. Lett.*, **88**, 243504 (2006).
15. A. S. Kushch, J. C. Bass, S. Ghamaty, and N. B. Eisner, in *Proceedings of 20th International Conference on Thermoelectrics (ICT2001)*, p. 422 (2001).
16. S. B. Schaevitz, A. J. Franz, K. F. Jensen, and M. A. Schmidt, in *Transducers '01 Eurosensors XV*, p. 30, Springer, Berlin Heidelberg (2001).
17. *Waste Heat Recovery: Technology Opportunities in the US Industry*, BCS Incorporated. U.S. Depart. of Energy, (2008).
18. G. G. Yadav, J. A. Susoreny, G. Zhang, H. Yang, and Y. Wu, *Nanoscale*, **3**, 3555 (2011).
19. D. Boutin and M. Bourgon, *Can. J. Chem.*, **39**, 915 (1961).
20. J. S. Anderson and M. C. Morton, *Proc. R. Soc. London A*, **184**, 83 (1945).
21. E. A. Dancy and G. J. Derge, *Trans. Metall. Soc. AIME*, **227**, 1033 (1963).
22. M. Bourgon, G. J. Derge, and G. M. Pound, *J. Met.*, **209**, 1454 (1957).
23. G. Handfield, M. D'Amboise, and M. Bourgon, *Can. J. Chem.*, **44**, 853 (1966).
24. M. Cutler and C. E. Mallon, *Phys. Rev.*, **144**, 642 (1966).
25. C. E. Mallon and M. Cutler, *Philos. Mag.*, **11**, 667 (1965).
26. Y. Nakamura and M. Shimoji, *Trans. Faraday Soc.*, **65**, 1509 (1969).
27. M. Cutler and C. E. Mallon, *J. Chem. Phys.*, **37**, 2677 (1962).
28. M. Cutler and C. E. Mallon, *J. Appl. Phys.*, **36**, 201 (1965).
29. E. A. Dancy, R. L. Pastorek, and G. J. Derge, *Trans. Metall. Soc. AIME*, **233**, 1645 (1965).
30. D. P. Belotskii and O. N. Manik, *J. Thermoelectr.*, **1**, 32 (2004).
31. R. K. Williams, M. Veeraburus, and W. O. Philbrook, *Metall. Trans.*, **3**, 255 (1972).
32. P. P. Shevchuk, V. V. Malinovskii, L. N. Aleksandrova, V. F. Zinchenko, and A. A. Velikanov, *Izv. Akad. Nauk SSSR. Neorg. Mater.*, **12**, 2064 (1976).
33. E. W. Johnson and R. L. Readal, *Adv. Energy Convers.*, **3**, 407 (1963).
34. J. W. Johnson, *Thermoelectric Materials Report No. 20*, Stanford Research Institute, (1962).
35. E. W. Johnson and R. L. Readal, *Adv. Energy Convers.*, **2**, 3 (1962).
36. Mineral Commodities Summary, U.S. Department of the Interior. U.S. Geological Survey (2016).
37. N. F. Mott, *Adv. Phys.*, **16**, 49 (1967).
38. A. F. Ioffe and A. R. Regel, in *Progress in Semiconductors*, vol. **4**, p. 237, John Wiley & Sons Inc., New York, NY (1960).
39. J. W. Johnson, *Thermoelectric Materials Report No. 21*, Stanford Research Institute (1962).
40. J. C. Johnson, *Thermoelectric Materials*, Report No. 22, Stanford Research Institute (1962).
41. A. R. Regel, I. A. Smirnov, and E. V. Shadrichev, *Phys. Status Solidi*, **5**, 13 (1971).
42. R. K. Williams, M. Veeraburus, and W. O. Philbrook, *Rev. Sci. Instrum.*, **39**, 1104 (1968).
43. V. M. Glazov, S. N. Chizhevskaya, and N. N. Glagoleva, *Liquid Semiconductors*, Plenum Press, New York, NY, (1969).
44. Q. Tan, L. Zhao, J. Li, C. Wu, T. Wei, Z. Xing, and M. G. Kanatzidis, *J. Mater. Chem. A*, **2**, 17302 (2014).
45. Q. Tan and J. Li, *J. Electron. Mater.*, **43**, 2435 (2014).
46. G. Ding, G. Gao, and K. Yao, *Sci. Rep.*, **5**, 9567 (2015).
47. W. Wijesekara, L. Rosendahl, D. R. Brown, and G. J. Snyder, *J. Electron. Mater.*, **44**, 1834 (2014).
48. J. E. Enderby and A. C. Barnes, *Rep. Prog. Phys.*, **53**, 85 (1990).
49. G. S. Nolas and H. J. Goldsmid, in *Thermal Conductivity - Theory, Properties, and Applications*, T. M. Tritt, Editor, p. 105, Plenum Publishers, New York, NY (2004).
50. F. E. Geiger and F. G. Cunningham, *Am. J. Phys.*, **32**, 336 (1964).
51. P. J. Price, *London, Edinburgh, Dublin Philos. Mag. J. Sci.*, **46**, 1252 (1955).
52. H. J. Goldsmid, *Proc. Phys. Soc. Sect. B*, **69**, 203 (1956).
53. C. Rinzler and A. Allanore, *Philos. Mag.*, **96**, 3041 (2016).